

Article

Radiation Balance and Partitioning of Latent and Sensible Heat Fluxes Over a Lime Orchard in Eastern Amazon

João Vitor de Nóvoa Pinto¹ , Deborah Luciany Pires Costa²,
Hildo Giuseppe Garcia Caldas Nunes¹, Alberto Cruz da Silva Junior¹,
Adriano Marlisom Leão de Sousa¹, Paulo Jorge de Oliveira Ponte de Souza¹,
Samuel Ortega-Farias³

¹Universidade Federal Rural da Amazônia, Belém, PA, Brazil.

²Instituto Internacional de Educação do Brasil, Belém, PA, Brazil.

³Universidad de Talca, Talca, Chile.

Recebido em: 14 de Agosto de 2022 - Revisado em: 23 de Outubro de 2022 - Aceito em: 23 de Novembro de 2022

Abstract

We investigate the balance of radiation and energy over a lime orchard in Eastern Amazon and how it relates to environmental conditions. We found that lime trees aged between 6 and 7 years old reflect 11.0% to 14.5% of incoming shortwave radiation, and the latent heat flux corresponds to 57.6% and 66.6% of the daily net radiation in the dry season (August - November) of 2020, and 2021, respectively. The soil heat flux represents 1% to 2% of the daily net radiation. Evapotranspiration was much lower than the reference evapotranspiration from August to November in 2019 and 2020. Evapotranspiration increased proportionally to the reference evapotranspiration from August to November 2021. This increase may be explained by weather conditions, such as the frequent rainfall during the dry season of 2021, in the same period when the energy for evapotranspiration is higher. Also, the high relative humidity between August and November 2021 may have favored the opening of stomata, increasing the orchard's evapotranspiration. The crop coefficient ranges between 0.74 and 0.84.

Palavras-chave: evapotranspiração, energia, saldo de radiação, razão de Bowen, recursos hídricos, região equatorial.

Balanco de Radiação e Partição de Fluxos de Calor Sensível e Latente Sobre Um Pomar de Lima Ácida na Amazônia Oriental

Resumo

Investiga-se o balanço de radiação e energia sobre um pomar de limão na Amazônia Oriental e como ele se relaciona com as condições ambientais. Foi descoberto que a lima ácida Tahiti com idades entre 6 e 7 anos refletem de 11,0% a 14,5% da radiação de ondas curtas recebidas, e o fluxo de calor latente corresponde a 57,6% e 66,6% do saldo de radiação diária nos períodos secos (agosto a novembro) de 2020 e 2021, respectivamente. O fluxo de calor do solo representa de 1% a 2% do saldo de radiação diário. A evapotranspiração foi muito menor que a evapotranspiração de referência de agosto a novembro em 2019 e 2020. A evapotranspiração aumentou proporcionalmente à evapotranspiração de referência de agosto a novembro de 2021. Esse aumento pode ser explicado pelas condições climáticas, como as chuvas frequentes durante o período seco de 2021, no mesmo período em que a energia para evapotranspiração é maior. Além disso, a alta umidade relativa entre agosto e novembro de 2021 pode ter favorecido a abertura dos estômatos, aumentando a evapotranspiração do pomar. O coeficiente de cultura variou entre 0,74 e 0,84.

Keywords: evapotranspiration, energy, net radiation, Bowen ratio, water resources, equatorial region.

1. Introduction

Water availability, air temperature, relative humidity, and solar irradiance are some of the various factors related

to the radiation balance and the partitioning of available energy between sensible and latent heat fluxes (Bagley *et al.*, 2017). Solar irradiance is the driving force behind most natural phenomena on Earth, and often the major

source of energy in various ecosystems and agroecosystems. As such, the Sun usually provides most of the energy available for evapotranspiration. As the amount of water available in the soil decreases, more of the available energy is used to heat the surface and the layer of air above it (Tang *et al.*, 2014).

The Amazon Region is supplied by large amounts of rainwater; however, precipitations are not homogeneous throughout the year. In Eastern Amazon, the second half of the year is usually hotter and drier than the first one (Amanajás and Braga, 2012), therefore, both temporary and permanent crops may experience water deficit, and irrigation is often needed to increase the fruit yield (Brum *et al.*, 2021). Furthermore, climate changes are expected to increase the average temperature and shorten the wet season in some places of the Eastern Amazon (Souza *et al.*, 2016). Therefore, to achieve more sustainable production and more efficiency in water usage the balance of energy and radiation must be known, particularly for irrigated crops and orchards.

The state of Pará, located in the Eastern Brazilian Amazon, is the second largest producer of “Tahiti” limes in Brazil (Instituto Brasileiro de Geografia e Estatística, 2020) and irrigation has been practiced in lime orchards in this region throughout the previous decade. The production of Tahiti lime in Pará surpassed 150,000 t in 2020, and Tahiti lime corresponds to more than 25% of the citrus production in this state. There are published results about the energy balance of citrus in scientific literature and even though many concepts related to the energy partitioning can be extrapolated for various regions and climate conditions, some are quite specific and dependent on management practices and land cover (Bagley *et al.*, 2017), such as the surface albedo (Vanomark *et al.*, 2018). Most research on radiation balance for limes are carried out in different regions and management practices, and their results differ largely. The current research was carried out in a Tahiti lime orchard with high density where trees were grafted onto citrumelo Swingle. These are uncommon management practices in this region.

This work aims to describe the seasonal variations of radiation balance and energy partitioning over a lime orchard in the state of Pará, and how they relate to weather conditions between 2019 and 2021.

2. Material and Methods

The experiment was carried out in a 12.5 ha Tahiti lime orchard (Fig. 1C) located in Eastern Amazon (1°48'19" S 47°11'52" W), in the municipality of Capitão Poço, state of Pará, Brazil (Fig. 1A and B). The wind rose in the figure below (Fig. 1C) shows the direction the wind comes from. The longest bar has a length equivalent to 200 m (Fig. 1C). The tower with all the instruments was

installed 100 m from the northern side and 80 m from the western side of the orchard.

The climate of this region is Am according to Köppen's climate classification (Alvares *et al.*, 2013). The mean annual rainfall in the previous decade (2011-2020) was above 2000 mm year⁻¹ according to the data recorded in the weather station of the Instituto Nacional de Meteorologia (INMET) located in the same municipality. The average weather conditions of each month in the decade 2011-2020 (the period with available weather measurements in this region) is shown in Table 1.

The three rainiest months are from January until March, when roughly 45% of the annual rainfall occurs. The three driest months are between August and October, when roughly 8% of the annual rainfall occurs. The mean annual temperature is 27.2 °C. November is the hottest month (28.1 °C), and July is the coldest one (26.6 °C). Mean relative humidity is above 68% in all months. Solar irradiance is higher during the dry season, due to low cloudiness. During the second half of the year, particularly between July and October, non-irrigated crops may experience some water deficit, due to the low precipitation and relative humidity associated with high air temperature and global radiation, which increases evapotranspiration (Allen *et al.*, 1998).

The orchard was surrounded by orange trees of various ages. Lime trees were planted in rows 6.8 m apart from each other. Plants in the same row are 2.0 m apart from its neighbors. Rows are aligned East-West. The 12.5 ha orchard is 500 m long in the East-West direction and 250 m long in the North-South direction. The orchard is irrigated during the driest months (usually from August until November), but in 2021, irrigation was not performed. The irrigation is performed every day by the company, except after heavy rains, and is equivalent to 5 mm day⁻¹ between August and November. During the period of the experiment between August 2020 and November 2020, the decision on whether to irrigate was based on the soil moisture read with tensiometers (as described below).

The soil moisture was estimated with the soil water retention curve (Genuchten, 1980) using the soil matric potential read with tensiometers installed at 30 cm depth, which is halfway the depth of the root system. In 2020, only four tensiometers were used, but it was increased to 12 tensiometers in July 2021. The 12 tensiometers were positioned aligned with the rows of plants and 1 m apart from the two neighbor trees. A water balance following the guidelines of FAO 56 (Allen *et al.*, 1998) was performed, considering an actual root depth of 0.6 m, an average height of lime trees of 4.0 m, and a fraction of soil covered by the canopy of 0.6 (dimensionless). The total available water was considered as 78 mm based on the field capacity and permanent wilting point of the area, obtained through the soil water retention curve.

For the calibration of the soil water retention curve, undeformed soil samples were obtained from 4 different points in the orchard, for each 10 cm of soil depth until 1 m. The undeformed soil samples were exposed to tensions of 1, 2, 4, 6, 10, 50, 100, 500, 1000, and 1500 kPa and the remaining moisture was measured by weighing the samples with a high precision scale. The van Genuchten equation (Genuchten, 1980) (Eq. (1)) was then fitted to the data obtained in this procedure.

$$\theta = \theta_r + \frac{\theta_s - \theta_r}{(1 + |\alpha h|^n)^m} \quad (1)$$

where: θ - soil moisture; θ_r , θ_s - residual and saturated soil moisture, respectively; h - tension read with the tensiometer; α , n , m - fitting parameters for the van Genuchten equation.

Sensors of air temperature and relative humidity were installed at 0.5 m and 2.0 m above the canopy of the trees, in the tower with instruments described previously (Fig. 1). A four-component net radiometer model CNR4 from Campbell Scientific was installed 2 m above the canopy and measurements of incoming (downward) and reflected shortwave radiation, as well as downward and upward components of longwave radiation were taken from May 2019 to March 2022. The 4-component net radiometer's pyranometers measure longwave radiation within a wavelength ranging from 4.5 μm to 42 μm . A NR-Lite net radiometer (Kipp & Zonen) was installed in another location in the same orchard between May 2019 and October 2020, so the integrity of the data could be assessed through the comparison of both measurements.

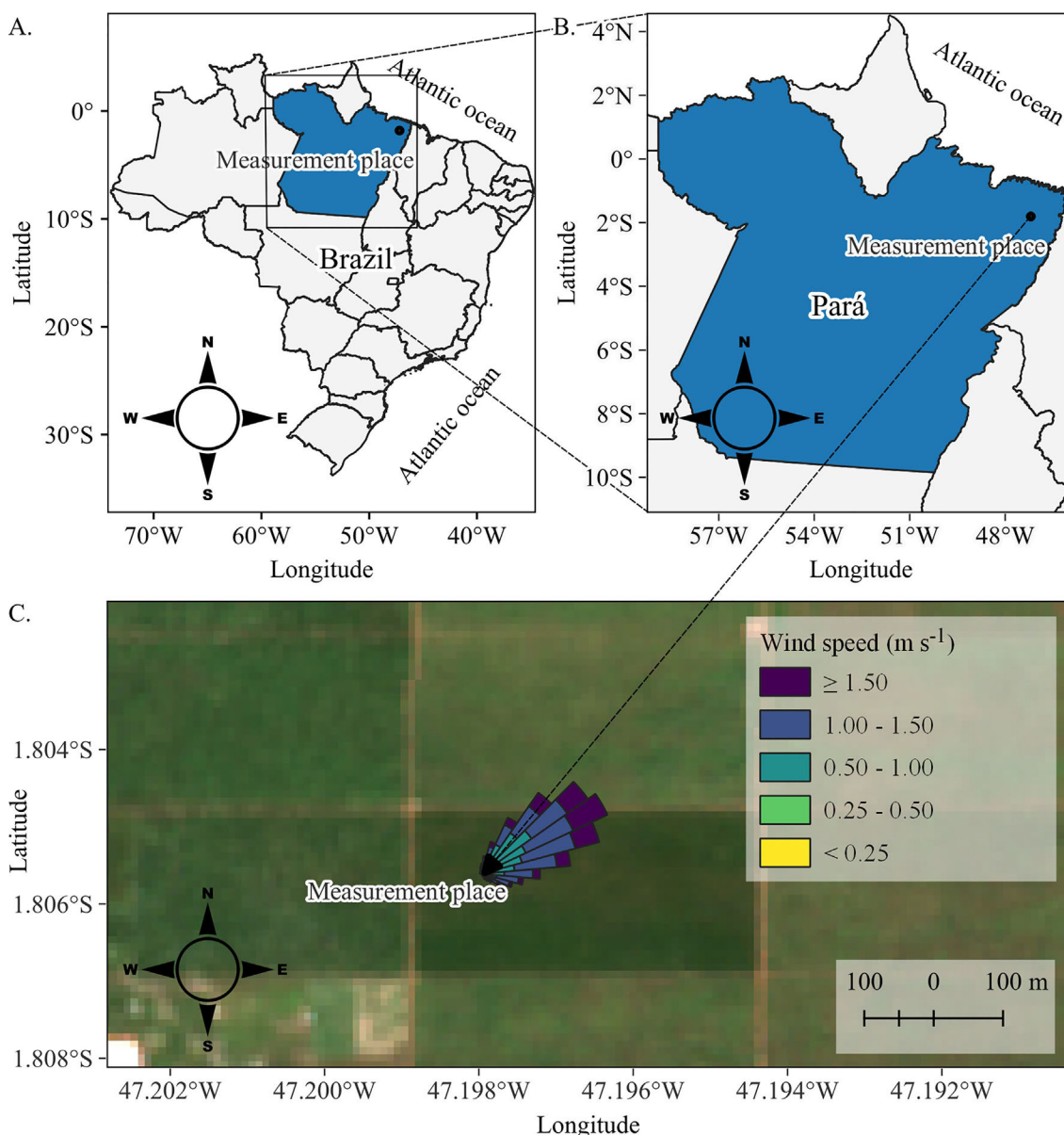


Fig. 1 - Map of the experiment and its location in the Brazilian territory.

Table 1 - Average weather conditions measured from 2011 to 2020 on the weather station of the National Institute of Meteorology located in Capitão Poço, PA, Brazil.

Month	Air temperature (°C)	Relative humidity (%)	Global radiation (MJ m ⁻² day ⁻¹)	Precipitation (mm)
January	27.1	75.4	14.1	356
February	26.9	77.6	13.7	506
March	26.8	78.5	13.9	286
April	27.0	78.0	14.8	202
May	27.1	77.2	17.1	175
June	26.8	75.8	16.1	152
July	26.6	74.8	18.0	75
August	26.9	72.5	19.7	13
September	27.5	70.8	18.6	31
October	27.9	69.0	18.1	44
November	28.1	68.7	17.1	107
December	27.8	70.5	15.2	111
Year	27.2 (average)	74.0 (average)	16.4 (average)	2058 (total)

Net radiation between the rows of lime trees was measured by a third net radiometer, model NR-Lite (Kipp & Zonen). Two plates for the measurement of soil heat flux (Hukseflux HFP01) were installed at a 10 cm depth, one between rows and another one in the rows of trees.

Net shortwave (R_{ns}) is regarded as the difference between incoming and reflected shortwave radiation (Eq. (2)), and net longwave radiation flux (R_{nl}) is the difference between downward and upward longwave radiation (Eq. (3)). Net radiation (R_n) is the sum of both R_{ns} and R_{nl} (Eq. (4)) (Allen *et al.*, 1998).

$$R_{ns} = S_{\downarrow} - S_{\uparrow} \quad (2)$$

$$R_{nl} = L_{\downarrow} - L_{\uparrow} \quad (3)$$

$$R_n = R_{ns} + R_{nl} \quad (4)$$

Due to malfunctioning of the temperature sensor of the 4-component net radiometer, the measured components of net longwave radiation (R_{ns} and R_{nl}) have a shift from the actual values. However, it does not affect the calculated net longwave radiation, since the subtraction referred above (Eq. (3)) cancels the temperature-dependent terms of net longwave measurements (Campbell Scientific Inc., 2021).

Albedo (α) is the ratio of reflected to incoming shortwave radiation (Eq. (5)) (Allen *et al.*, 1998).

$$\alpha = \frac{S_{\uparrow}}{S_{\downarrow}} \quad (5)$$

Albedo was calculated by a linear regression between S_{\downarrow} as explanatory variable and S_{\uparrow} as response variable, with the intercept set to 0. Therefore, albedo is the slope of such equation. Regression analysis was performed to assess the reliability and uncertainty of the calculated albedo.

Latent (H) and sensible heat (λE) fluxes were calculated over one year through the Bowen Ratio Energy Balance (BREB) method. Bowen ratio (β) is defined as the ratio of sensible to latent heat flux (Eq. (6)), which can be calculated from measurements of air temperature and water vapor pressure at different heights under certain conditions (Perez *et al.*, 1999).

$$\beta = \frac{H}{\lambda E} = \frac{p_a c_p}{\lambda \varepsilon} \left(\frac{k_h}{k_v} \right) \frac{\delta T / \delta z}{\delta e / \delta z} = \gamma \left(\frac{k_h}{k_v} \right) \frac{\delta T / \delta z}{\delta e / \delta z}, \quad (6)$$

where k_v and k_h - coefficients for turbulent diffusion of water vapor and sensible heat; $\varepsilon = 0.622$ - ratio of molecular weight of water to molecular weight of dry air; p_a - atmospheric pressure; c_p - specific heat of air at constant pressure; λ - latent heat of vaporization of water; $\gamma = p_a c_p / \lambda \varepsilon$ - psychrometric constant; T - air temperature; and e - pressure of water vapor. Given $k_v = k_h$ for adiabatic conditions, it results in the simplified equation (Eq. (7))

$$\beta = \gamma \frac{\Delta T}{\Delta z}, \quad (7)$$

where ΔT - difference in temperature between measurement heights z_1 and z_2 ; and Δe - vapor pressure difference between heights z_1 and z_2 . The energy balance equation for a uniform surface is

$$R_n = H + G + \lambda E. \quad (8)$$

where G is the soil heat flux.

From Eqs. (8) and (6) the following relation arises

$$\lambda E = \frac{R_n - G}{1 + \beta}, \quad (9)$$

where: λ - latent heat of vaporization of water; and E - evapotranspiration. Finally, H can be obtained as the residual of R_n when R_n , G and λE are known.

Since BREB is unstable when β approaches -1, the objective criteria for rejecting Bowen Ratio results described by Perez *et al.*, (1999) was applied to the results of the calculations above. Negative values of λE were disregarded on the computation of the total daily evapotranspiration, even though they are kept for the computation of energy fluxes. After the data was filtered according to the above criteria, the latent heat flux for the gaps originated from the filtering was predicted by multiple linear regression with all the measured variables. For comparison purposes, daily reference evapotranspiration (ET_0) was calculated with the standard FAO Penman-Monteith (Allen *et al.*, 2006) method with data from a standard weather station located 17 km away from the experiment site. The actual daily evapotranspiration obtained by summing the hourly E (Eq. (9)) of each day was compared with the reference evapotranspiration and the crop coefficient was fitted (Eq. (10)) (Allen, *et al.*, 1998),

$$ET = K_c ET_0, \quad (10)$$

where: ET - daily actual evapotranspiration, ET_0 - reference evapotranspiration, and K_c - crop coefficient, obtained by linear regression.

Furthermore, gas exchange measurements were performed in October 2020. Carbon assimilation rate (A), stomatal conductance (g_s), and transpiration (E) were measured in 15 plants randomly chosen in the orchard. Measurements were made in leaves found near halfway the distance from the bottom to the top of the canopy. Such results are used to explain some of the observations discussed throughout this work.

Regarding the figures and calculations in the current study, the map (Fig. 1) was made with QGIS v3.22, and the other figures, calculations and statistics were made with R v4.2.

3. Results and Discussion

Incoming shortwave radiation reaches up to 25 MJ $m^{-2} day^{-1}$ on some days during the dry seasons (August - November) of 2019 and 2020, and values as low as 5 MJ $m^{-2} day^{-1}$ during the wettest months (February - April) of 2021 (Fig. 2A). There is a noticeable difference between the dry season (August - November) of 2020 and the dry season (August - November) of 2021 when the recorded downward shortwave radiation was lower than in previous

years (i.e., 2019, and 2020). Such differences seem to be related to the occurrence of La Niña of moderate intensity that begins with the onset of the rainy season in the second half of October 2020 (National Oceanic and Atmospheric Administration, 2022). La Niña is usually related to increased rainfall in the Amazon (MOURA *et al.*, 2019), which explains the high amount of rainfall during the dry season (August - November) of 2021 (Fig. 2C), as well as the cloudier conditions (compared to the previous dry season) in the same period. Cloudiness is one of the most important factors that influence the amount of global radiation in this region, and it exerts a significant influence on radiation balance as demonstrated in other studies (Eltahir and Humphries Júnior, 1998).

The lower cloudiness and higher downward shortwave radiation (Fig. 2A) caused the air temperature to reach peaks above 35 °C during September 2020 (Fig. 2B), and relative humidity was as low as 55% during the driest months, with mean relative humidity below 80% on some days. The same period in 2021 recorded relative humidity above 80% and minimum relative humidity usually above 60%. As a result, vapor pressure deficit reached highest daily average values in 2019 and 2020 than in 2021 (Fig. 2D), the same occurs with wind speed (Fig. 2E), which is also an important determinant of evapotranspiration. The soil moisture remained high from August until November 2020, due to the irrigation (Fig. 3).

Tensiometers indicated that the soil was much drier during the dry season (August - November) of 2021 than during the dry season (August - November) of 2020, even though the dry season of 2021 was rainier. The precipitation data shows that the rainfall of the dry season (August - November) of 2021 was distributed among various events of small rainfall - a little above 13 mm (Fig. 2). This situation increases the interception of water by the canopy of trees since the canopy is initially dry and needs to be saturated before the water can reach the underneath soil (Távora and Koide, 2020).

Regarding the variations of the radiation balance between seasons, it has been seen that during the wet months (usually between December and May), the global radiation reaches is between 650 and 750 $W m^{-2}$ at noon (local time), whereas, during the dry season, from September to November, the mean incoming shortwave radiation at local noon is above 750 $W m^{-2}$ (Fig. 4).

Due to the proximity to the equator, this region does not have great variations of incoming extraterrestrial radiation (R_a) throughout the year. R_a reaches 32.6 MJ $m^{-2} day^{-1}$ in July, and 38.0 MJ $m^{-2} day^{-1}$ in March. During the wet season, S_{\downarrow} measured between 9 h and 12 h (local time) is about 50% to 60% of extraterrestrial radiation R_a . After 13 h, incoming shortwave radiation is less than 50% of R_a , which indicates higher cloudiness during these hours. Between August and September, the frequency of clear-sky conditions is higher. During these months, the mean S_{\downarrow}

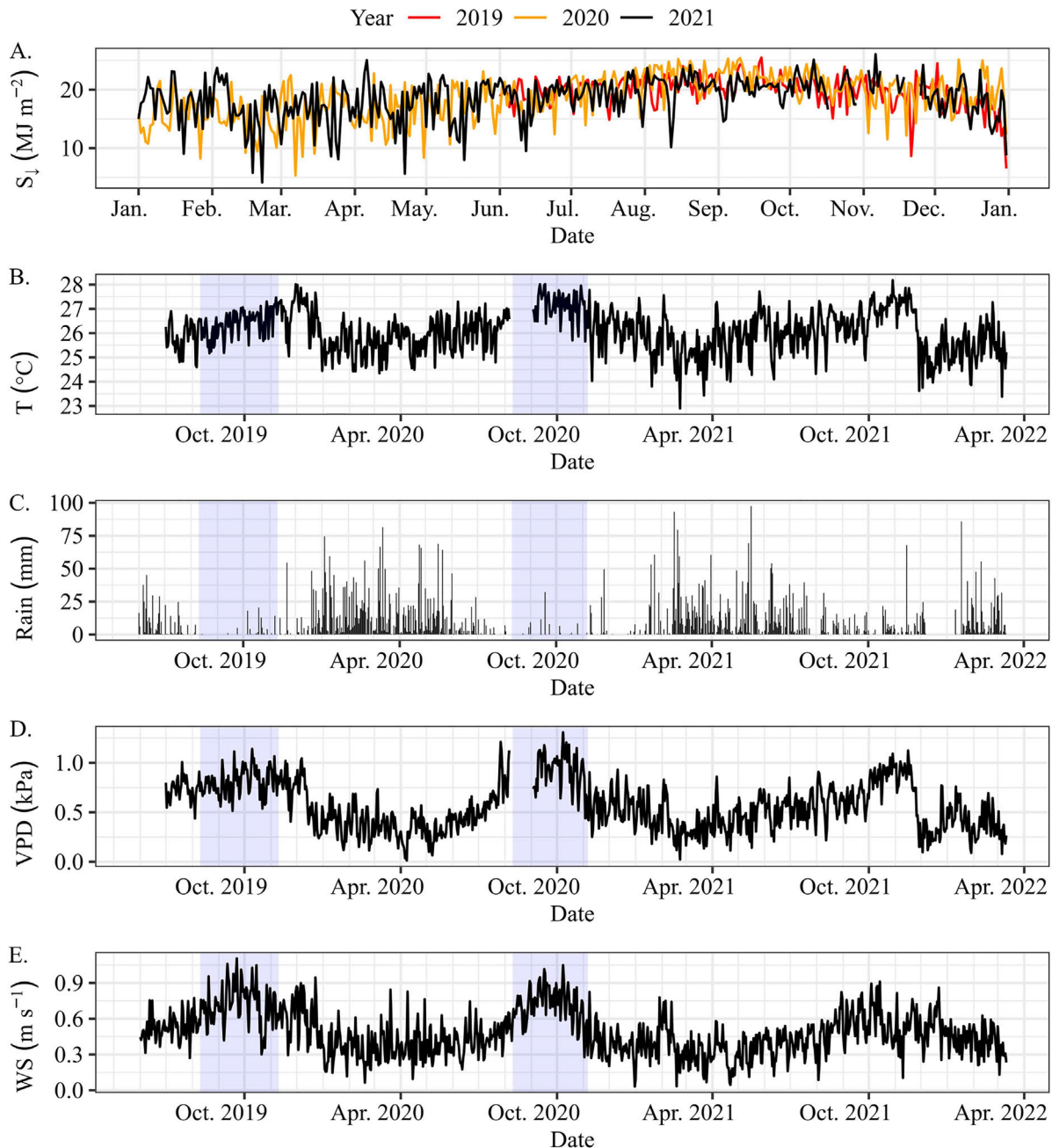


Fig. 2 - Variation of weather variables between 2019 and 2021 in the lime orchard. The gray area in the plot of air temperature shows the range between minimum and maximum daily relative air temperature. The blue area shows the irrigated periods for 2019 and 2020. S_i - incoming shortwave radiation; T - Air temperature; VPD - vapor pressure deficit; WS - wind speed.

between 8 h and 14 h (local time) is between 60% and 70% of R_q . Cloudiness is therefore one of the factors responsible for differences in the radiation balance between the dry and the wet season.

Net longwave radiation is more negative between August and October, when the average R_{nl} is -50 W m^{-2} during the hottest hours of the day. A more negative net longwave radiation could be related to the warming of the surface caused by the higher incidence of downward

shortwave radiation and lower water availability as well as the reduced cloudiness during the dry season. Clouds impact the radiation balance by reflecting shortwave radiation and emitting longwave radiation (Nyeki *et al.*, 2019), so they contribute to increase the net longwave radiation (making it less negative), while the heating of the surface increases the emissions of longwave radiation upwards. During the dry season, air temperature is also higher than in the other months because of the warmer

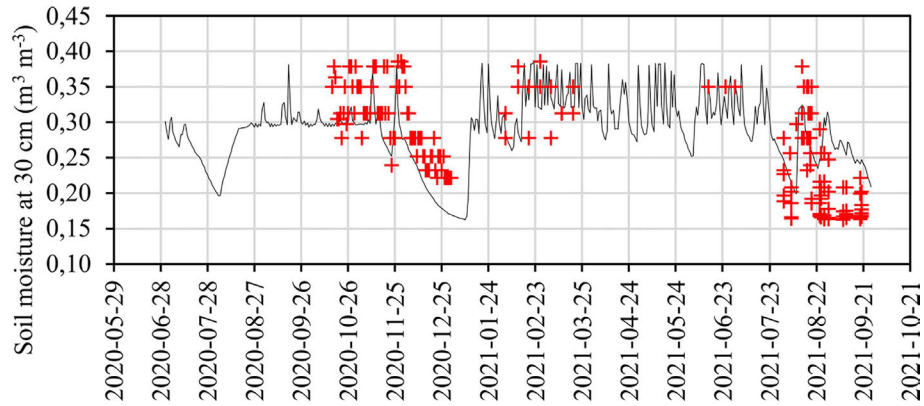


Fig. 3 - Variation of soil moisture from September 2020 to September 2021. Points represent measurements with tensiometers, and the line is the soil moisture simulated by a water balance.

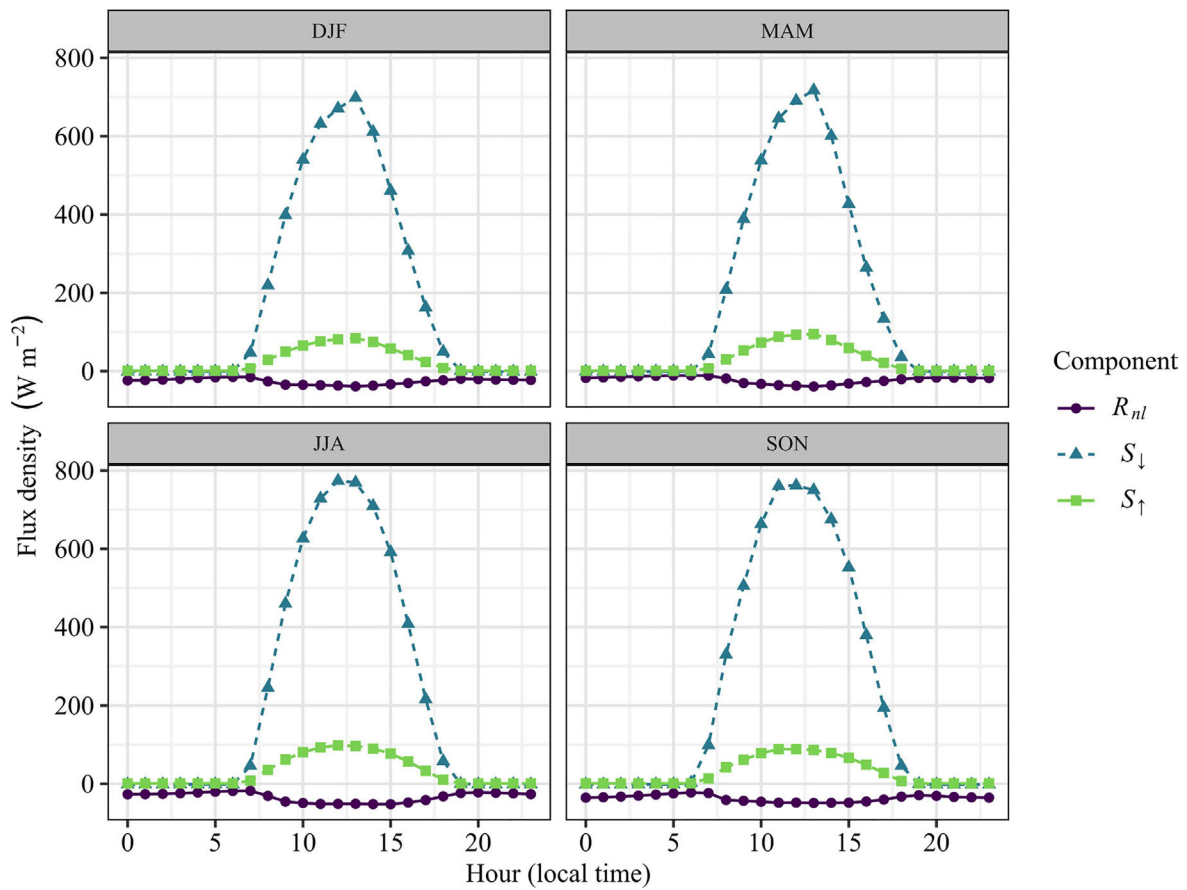


Fig. 4 - Average incoming shortwave radiation (S_{\downarrow}), reflected shortwave radiation (S_{\uparrow}), and net longwave radiation (R_{nl}) throughout the day in each month.

surface. At local noon, the mean air temperature measured 2.0 m above the canopy is higher than 32.5 °C during the dry season (Fig. 2).

3.1. Albedo

Albedo was calculated as $0.1276 \pm 7.611 \times 10^{-5}$ ($p < 0.01$) with two and a half years of measurements

(Fig. 5A, B). Albedo calculated between May 2021, and September 2021 was a little higher than the average of the same months in 2020, but it returned to the average in September (Fig. 5A). Albedo may also be influenced by the pruning of trees performed at the end of the first half of 2021, even though this event alone cannot explain the peak observed in 2021, since the

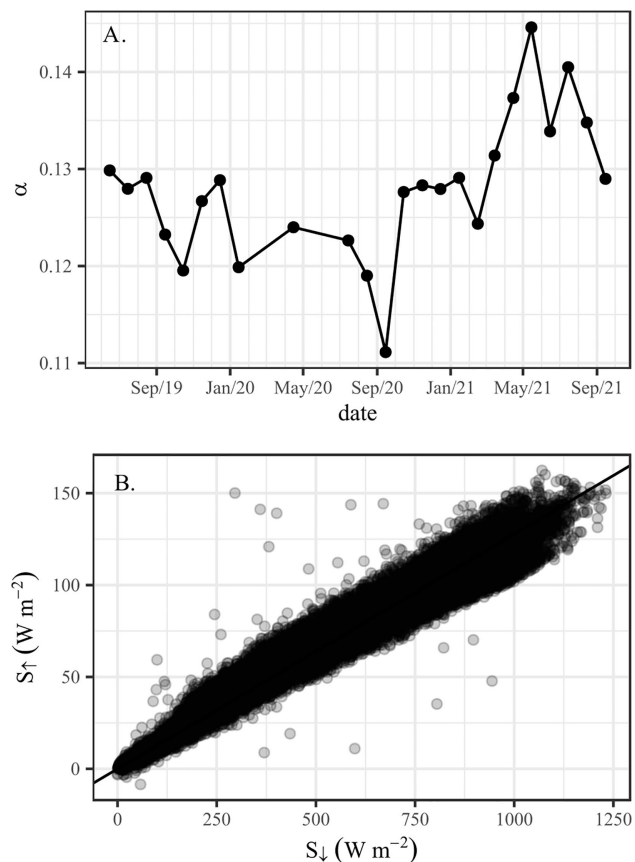


Fig. 5 - Variation of albedo per month from June - 2019 until September - 2021. Points in figure A represent the slope of the regression analysis between S_{\uparrow} and S_{\downarrow} performed for each month.

increase of albedo begins a few months before the pruning. The pruning may induce some variation of the surface albedo due to its effects on the leaf area index (the leaf area per unit of land area). Agricultural practices that change or modify the soil's coverage are likely to impact the albedo because they change the amount of solar radiation reaching the ground, and therefore, they impact the whole balance of energy (Liu *et al.*, 2022).

Despite the existence of peaks in measurements of albedo as shown in Fig. 5A, the variations are small, so a scatter plot using all the available 10 min measurements of S_{\downarrow} and S_{\uparrow} from 2019 to 2021 still shows a high positive correlation, with Pearson's correlation coefficient up to 0.99 (Fig. 5B), so it is not necessary to establish albedo values for each phenological stage or the dry and the wet seasons separately.

Reports of surface albedo were not found for lime orchards in the scientific literature for the past few years for comparison purposes, but the value found is a little smaller than the albedo of croplands and inside the range of values found for forest areas in the Amazon region (Faria *et al.*, 2018).

3.2. Latent and sensible heat fluxes

About 36% of the available data regarding Bowen Ratio calculations was excluded by the criteria outlined by Perez *et al.* (1999). During the months with lower rainfall in 2020 and 2021 (from July to October 2020/2021), 27% of the available data was excluded, whereas 40% was excluded during the wet season (all remaining months). Estimates of latent heat by means of the BREB method usually fail when negative temperature gradients occur during unstable conditions and nighttime, and when the inversion of flux directions occurs at the morning or evening (Perez *et al.*, 1999). Between December and June, rainfalls are very frequent (Fig. 2) and may occur several times a day, which leads to greater uncertainty of the calculated fluxes. This amount of excluded data is normal according to Perez *et al.* (1999), which indicates that on average, 40% of the data must be rejected, including mostly data obtained during irrigations, at night, and during rainfall events.

The variations observed in the daily pattern of latent, sensible, and soil heat fluxes throughout the year, were small. The sensible heat usually reaches its maximum between 10 h and 12 h (local time) and the latent heat flux usually reaches its maximum after the local noon. The maximum flux density of λE and H is usually around 400 W m^{-2} . During morning in the dry season (August - November) of 2020, H is greater than λE , then an inversion occurs at noon, when λE becomes greater than H . These are the only months with daily irrigation in the whole time series so this behavior might be related to the irrigation. Irrigation was not performed at the same time every day, but it usually begins in the afternoon, so an increase of soil moisture occurring at this time might explain why λE becomes greater than H in the afternoon in months with irrigation.

During the daytime, latent heat flux varies between 47.0% and 74.6% of R_n from September to October, and between 44.5% and 79.9% of R_n during the other months. The soil heat flux corresponds to 43.8% of R_n at nighttime between November and July, and 23.6% of R_n at night between August and October. During daytime, the soil heat flux usually represents as little as 1.7% of R_n . The total daily soil heat flux is usually between 1% and 2% of the total daily R_n , and the median of the latent heat flux was 57.6% of R_n during the irrigated months of 2020 (between August and October), 62.1% of R_n between November 2020 and July 2021, and 66.6% of R_n during the dry season of 2021 (August - September). Looking at the average flux density calculated for periods of three months (Fig. 6), there is a noticeable increase in the net radiation on the transition from the wettest months (March, April, May - MAM) to the driest months (September, October, November - SON).

The average λE during MAM was much higher than the H , which indicates that most of the available energy

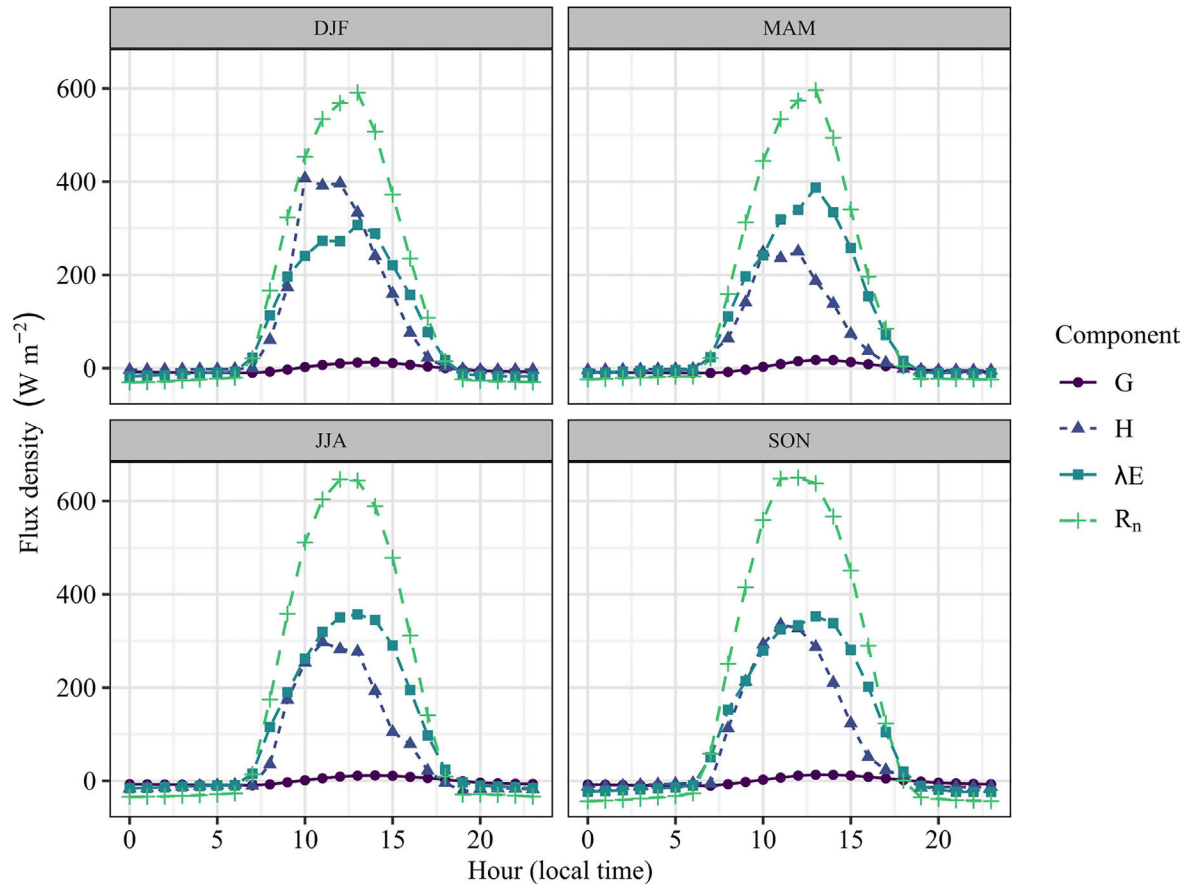


Fig. 6 - Mean hourly soil heat flux G , sensible heat flux H , latent heat flux λE and net radiation R_n calculated for each three-month period. DJF - December, January, and February; MAM - March, April, and May; JJA - June, July, and August; SON - September, October, and November.

during these months is being used for evapotranspiration. On the other hand, SON has the highest available energy, as demonstrated by the higher peak reached by the light green line (R_n) in Fig. 6, but the lower availability of rainwater in this period seems to inhibit the evapotranspiration, so λE does not increase by the same amount as (R_n), which means that relatively less of the total available energy was spent with evapotranspiration.

As shown in Fig. 7, the evapotranspiration found for Tahiti lime in the current research is usually lower than the reference evapotranspiration for the studied region. This is expected, as shown for various citric species worldwide. The increase of the evapotranspiration between August and November may be explained by higher atmospheric demand, due to the increase in the availability of energy caused by the increase of solar radiation in this period, higher air temperature and reduced relative humidity, as discussed previously. Another determinant factor for evapotranspiration is the availability of water, which was supplied through irrigation in 2019 and 2020 (see Fig. 2). However, as shown below (Fig. 7A), the actual evapotranspiration of the orchard is almost equal to the reference evapotranspiration between August 2021 and Novem-

ber 2021, despite the lack of irrigation and the soil being much drier in this period than during the then same months in 2020.

The increase of evapotranspiration in 2021 could be related to the higher occurrence of rains during the year. Even though the soil moisture estimated with tensiometers was lower in the dry season (August - November) of 2021 than in 2020, the tensiometers were installed below the canopy. This soil beneath the canopy is more easily reached by irrigation water than by rainwater because the canopy needs to be saturated before the water reaches the ground, as discussed previously. On the other hand, the rainwater wets the whole surface and, therefore, it may increase the evapotranspiration from interrow spaces, that are not reached by irrigation water. The same thing happens in the wet season, when there is not irrigation, but the evapotranspiration measured by the BREB method does not reduce as much as the reference evapotranspiration, due to the high amount of rainfall water in this region.

The crop coefficient K_c found for Tahiti lime was lower than 1 (Fig. 7B and C). Marin *et al.* (2016) found the K_c for Tahiti lime to range between 0.68 and 0.74 during summer, and Jamshid *et al.* (2020) found the K_c to range

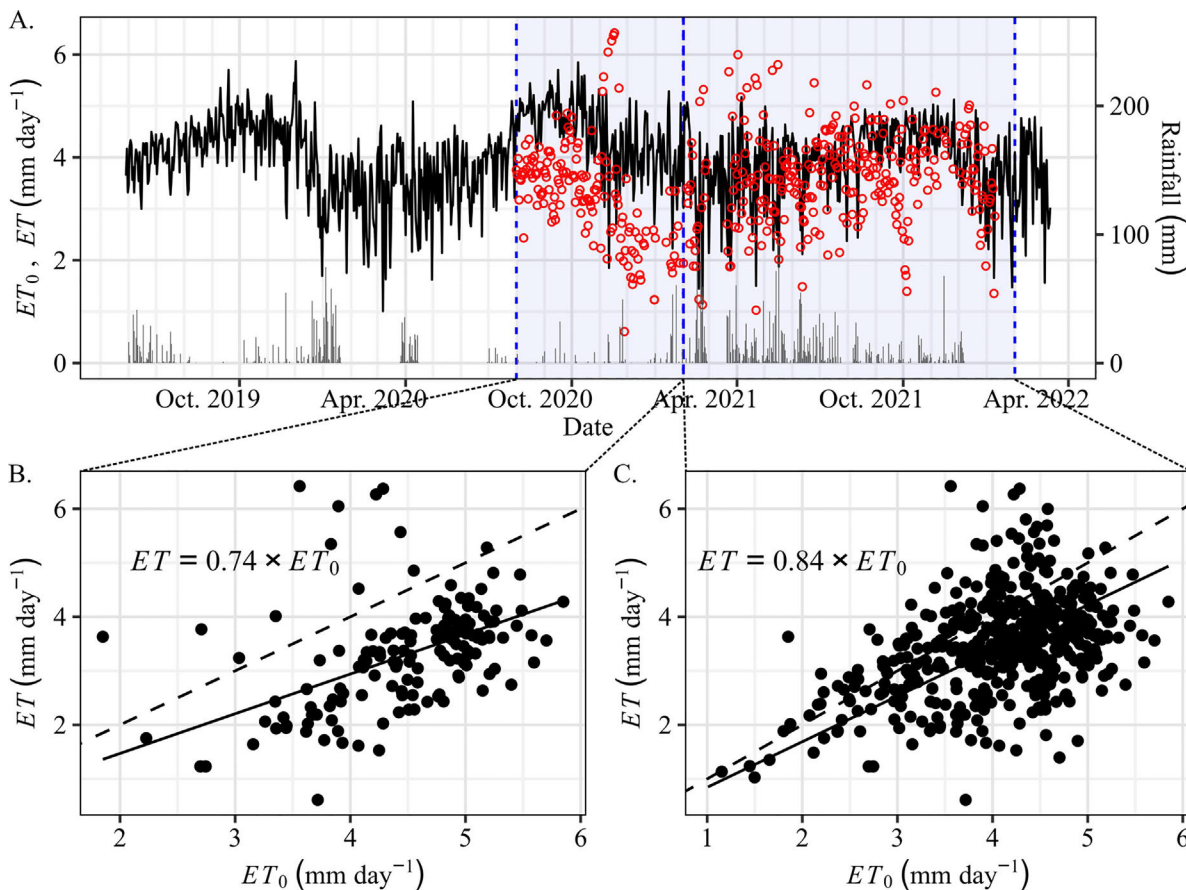


Fig. 7(A) - Comparison between actual evapotranspiration (ET , red points, left axis) and reference evapotranspiration (ET_0 , black line, left axis), with rainfall shown below (columns, right axis) from August 2020 until April 2022. **(B)** Comparison of actual evapotranspiration (ET , vertical axis) and reference evapotranspiration (ET_0 , horizontal axis) in the same day, with a continuous line showing the fitted equation and the dashed line showing the region where $ET_0 = ET$, between August 2020 and January 2021. **(C)** Same as **(B)**, but between February 2021, and January 2022. ET_0 : reference evapotranspiration; ET : actual evapotranspiration. The period before August 2020 lacks some data needed for the calculation of Bowen Ratio, so it was ignored in the analysis above.

between 0.67 and 0.97 for orange (*Citrus sinensis*). The low crop coefficient, even when the trees are well watered may be explained by the stomatal control of Tahiti lime. Citrus species tend to close their stomata when the vapor pressure deficit is higher than 1.5 kPa (Silva *et al.*, 2018; Ribeiro and Machado, 2007), even when water is not limited. Despite the measurements of gas exchange (Table 2) carried out in 2020 were obtained during early morning, the vapor pressure deficit was higher than 1.5 kPa at the time of the measurements, therefore it may be concluded that there was a stomatal control over evapotranspiration, even though the plants were being irrigated.

Even though the carbon assimilation rate was low, it is inside the normal range found for citric species CO_2

assimilation rate found in scientific literature for citrus in general. For *C. sinensis*, an assimilation rate below $15 \mu\text{mol CO}_2 \text{ m}^{-2} \text{ s}^{-1}$ has been found for plants with adequate nutritional management, and it decreased below $5 \mu\text{mol CO}_2 \text{ m}^{-2} \text{ s}^{-1}$ with Boron deficiency (Yang *et al.*, 2022). Furthermore, a maximum assimilation rate of $11.0 \mu\text{mol CO}_2 \text{ m}^{-2} \text{ s}^{-1}$ is reported for ‘Valencia’ orange trees during the summer in Piracicaba, southeastern Brazil (Ribeiro; Machado, 2007). Stomatal conductance (g_s) showed a huge variance, but the mean was similar to the mean g_s found for young acid lime trees by Mira-Garcia *et al.* (2021).

4. Conclusion

1. Even though the albedo has some variations throughout the measurement period, from 2019 to 2021, a value of 0.13 can be adopted for the whole period.
2. The uncertainty of the measured fluxes is higher during the wet season than during the dry season, due to the increased frequency of rains in the wet season.

Table 2 - Carbon assimilation rate (A), transpiration (E) and stomatal conductance (g_s) measured in Tahiti lime trees in October 2020.

A ($\mu\text{mol CO}_2 \text{ m}^{-2} \text{ s}^{-1}$)	E ($\text{mmol H}_2\text{O m}^{-2} \text{ s}^{-1}$)	g_s ($\text{mmol H}_2\text{O m}^{-2} \text{ s}^{-1}$)
9.51 ± 2.71	1.71 ± 0.65	94.4 ± 44.5

3. A slight increase of lime's evapotranspiration was seen between 2020, and 2021, even with no irrigation in 2021. The increase may be explained by the different weather conditions in 2021, with a higher frequency of rainfall events that increased the contribution of the vegetation between the rows of Tahiti limes to the total evapotranspiration.
4. The crop coefficient ranges between 0.74 and 0.84 under the current management and climate conditions.

References

- ALLEN, R.G.; PEREIRA, L.S.; RAES, D.; SMITH, M. **Crop Evapotranspiration: Guidelines for Computing Crop Water Requirements FAO Irrigation and Drainage Paper 56**. Rome: FAO, 1998.
- ALLEN, R.G.; PRUITT, W.O.; WRIGHT, J.L.; HOWELL, T.A.; VENTURA, F.V.; *et al.* A recommendation on standardized surface resistance for hourly calculation of reference ETo by the FAO56 Penman-Monteith method. **Agric. Water Manag.**, v. 81 n. 1-2, p. 1-22, 2006.
- ALVARES, C.A.; STAPE, J.L.; SENTELHAS, P.C.; MORAES, J.L.; SPAROVEK, G. Köppen's climate classification map for Brazil. **Meteorol. Z.**, v. 22, n. 6, p. 711-728, 2013.
- AMANAJÁS, J.C.; BRAGA, C.C. Padrões espaço-temporal pluviométricos na Amazônia Oriental utilizando análise multivariada. **Rev. Bras. Meteorol.**, v. 27, n. 4, p. 423-434, 2012.
- BAGLEY, J.E.; KUEPPERS, L.M.; BILLESBACH, D.P.; WILLIAMS, I.N.; BIRAUD, S.C.; *et al.* The influence of land cover on surface energy partitioning and evaporative fraction regimes in the U.S. Southern Great Plains. **J. Geophys. Res. Atmos.**, v. 22, n. 11, p. 5793-5807, 2017.
- BRUM, M.; OLIVEIRA, R.S.; LÓPEZ, J.G.; LICATA, J.; PYPKER, T.; *et al.* Effects of irrigation on oil palm transpiration during ENSO-induced drought in the Brazilian Eastern Amazon. **Agric. Water Manag.**, v. 245, 106569, 2021.
- CAMPBELL SCIENTIFIC INC. **CNR4 Net Radiometer Product Manual, rev. 6/2021**. Logan: Campbell Scientific Inc., 2021.
- ELTAHIR, E.A.B.; HUMPHRIES JÚNIOR., E.J. The role of clouds in the surface energy balance over the Amazon Forest. **Int. J. Climatol.**, v. 18, n. 14, p. 1575-1591, 1998.
- FARIA, T.O.; RODRIGUES, T.R.; CURADO, L.F.A.; GAIO, D.C.; NOGUEIRA, J.S. Surface albedo in different land-use and cover types in Amazon Forest region. **Rev. Ambiente Água**, v. 13, n. 2, e2120, 2018.
- GENUCHTEN, M.T.A. Closed-form equation for predicting the hydraulic conductivity of unsaturated soils. **Soil Sci. Soc. Am. J.**, v. 44, n. 5, p. 892-898, 1988.
- INSTITUTO BRASILEIRO DE GEOGRAFIA E ESTATÍSTICA. **Sistema IBGE de Recuperação Automática**. IBGE: Brasília, 2020.
- JAMSHIDI, S.; ZAND-PARSA, S.; KAMGAR-HAGHIGHI A.A.; SHAHSAVAR, A.R.; NIYOGLI, D. Evapotranspiration, crop coefficients, and physiological responses of citrus trees in semi-arid climatic conditions. **Agric. Water Manag.**, v. 227, 105838, 2020.
- LIU, J.; DESJARDINS, R.L.; WANG, S.; WORTH, D.E.; QIAN, B.; *et al.* Climate impact from agricultural management practices in the Canadian prairies: carbon equivalence due to albedo change. **J. Environ. Manag.**, v. 302, part A, 113938, 2022.
- MARIN, F.R.; ANGELOCCI, L.R.; NASSIF, D.S.P.; COSTA, L.G.; VIANNA, M.S.; *et al.* Crop coefficient changes with reference evapotranspiration for highly canopy-atmosphere coupled crops. **Agric. Water Manag.**, v. 163, p. 139-145, 2016.
- MOURA, M.M.; SANTOS, A.R.; PEZZOPANE, J.E.M.; ALEXANDRE, R.S.; SILVA, S.F.; *et al.* Relation of El Niño and La Niña phenomena to precipitation, evapotranspiration and temperature in the Amazon basin. **Sci. Total Environ.**, v. 651, n. 1, p. 1639-1651, 2019.
- MIRA-GARCIA, A.B.; VERA, J.; CONEJERO, W.; CONESA, M.R.; RUIZ-SÁNCHEZ, M.C. Evapotranspiration in young lime trees with automated irrigation. **Sci. Hortic.**, v. 288, 110396, 2021.
- NYEKI, S.; WACKER, S.; AEBI, C.; GRÖBNER, J.; MARTUCCI, G.; *et al.* Trends in surface radiation and cloud radiative effect at four Swiss sites for the 1996-2015 period. **Atmos. Chem. Phys.**, v. 19, p. 13227-13241, 2019.
- NATIONAL OCEANIC AND ATMOSPHERIC ADMINISTRATION. **Historical El-Niño/La-Niña Episodes (1950-Present)**. Washington, D.C.: NOAA, 2022.
- PEREZ, P.J.; CASTELLVI, F.; IBAÑEZ, M.; ROSELL, J.I. Assessment of reliability of Bowen ratio method for partitioning fluxes. **Agric. For. Meteorol.**, v. 97, n. 3, p. 141-150, 1999.
- RIBEIRO, R.V.; MACHADO, E.C. Some aspects of citrus eco-physiology in subtropical climates: re-visiting photosynthesis under natural conditions. **Braz. J. Plant Physiol.**, v. 19, n. 4, p. 393-411, 2007.
- SILVA, G.S.; GAVASSI, M.A.; NOGUEIRA, M.A.; HABERMANN, G. Aluminum prevents stomatal conductance from responding to vapor pressure deficit in Citrus limonia. **Environ. Exp. Bot.**, v. 155, p. 662-671, 2018.
- SOUZA, E.B.; CARMO, A.M.C.C.; MORAES, B.C.; NACIF, A.; FERREIRA, D.B.S.; *et al.* Sazonalidade da precipitação sobre a Amazônia Legal brasileira: clima atual e projeções futuras usando o modelo REGCM4. **Rev. Bras. de Climatologia**, v. 18, p. 293-306, 2016.
- TANG, Y.; SUN, X.; WANG, H. Interannual variation of the Bowen ratio in a subtropical coniferous plantation in Southeast China, 2003-2012. **Plos One**, v. 9, n. 2, e88267, 2014.
- TÁVORA, B.E.; KOIDE, S. Event-based rainfall interception modeling in a Cerrado Riparian Forest - Central Brazil: An alternative approach to the IS method for parameterization of the Gash model. **Water**, v. 12, n. 8, 2128, 2020.
- VANOMARK, G.M.M.S.; ESPÍNOLA SOBRINHO, J.; BEZERRA, J.R.C.; SANTOS, C.A.C.; *et al.* Energy balance partitioning and evapotranspiration from irrigated Muskmelon under Semi-Arid conditions. **Agronomy**, v. 77, n. 1, p. 168-180, 2018.
- YANG, L.; PAN, J.; HU, N.; CHEN, H.; JIANG, H.; *et al.* Citrus physiological and molecular response to boron stresses. **Plants**, v. 11, n. 1, 40, 2022.

Internet resources

INSTITUTO BRASILEIRO DE GEOGRAFIA E
ESTATÍSTICA. <https://sidra.ibge.gov.br/>
NATIONAL OCEANIC AND ATMOSPHERIC
ADMINISTRATION. [https://origin.cpc.ncep.noaa.gov/pro
ducts/analysis_monitoring/ensostuff/ONI_v5.php](https://origin.cpc.ncep.noaa.gov/products/analysis_monitoring/ensostuff/ONI_v5.php)

License information: This is an open-access article distributed under the terms of the Creative Commons Attribution License (type CC-BY), which permits unrestricted use, distribution and reproduction in any medium, provided the original article is properly cited.